

AD-A169 466

COORDINATED RADAR AND SATELLITE STUDIES OF IONOSPHERIC
CURRENTS IN THE AU. (U) SRI INTERNATIONAL MENLO PARK CA
R T TSUNODA ET AL. DEC 85 AFGL-TR-86-0022

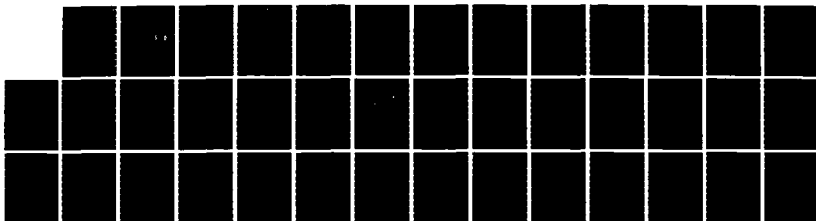
1/1

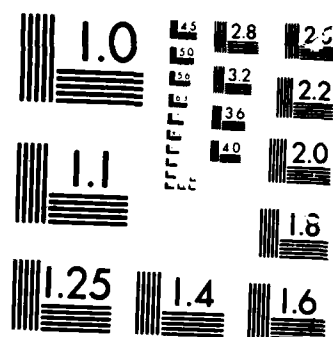
UNCLASSIFIED

F19628-02-K-0045

F/G 4/1

NL





VERBODEN

100%

AFGL-TR-86-0022

**COORDINATED RADAR AND SATELLITE STUDIES
OF IONOSPHERIC CURRENTS IN THE AURORAL ZONE
AND POLAR CAP**

By: ROLAND T. TSUNODA ANNE Q. SMITH JOHN D. KELLY
ROBERT M. ROBINSON

SRI INTERNATIONAL
333 Ravenswood Avenue
Menlo Park, California 94025

December 1985

Final Report
For Period 1 September 1982 -- 31 December 1985

DTIC
ELECTE
JUL 01 1986
S D

APPROVED FOR PUBLIC RELEASE. DISTRIBUTION UNLIMITED.

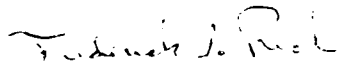
Prepared for: AIR FORCE GEOPHYSICS LABORATORY
AIR FORCE SYSTEMS COMMAND
UNITED STATES AIR FORCE
HANSCOM AIR FORCE BASE, MASSACHUSETTS 01731

AD-A169 466

DTIC FILE COPY


SAMPLE FOR CONTRACTOR REPORTS

"This technical report has been reviewed and is approved for publication"



(Signature)

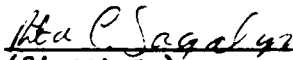
FREDERICK J. RICH
Contract Manager



(Signature)

NELSON MAYNARD
Branch Chief

FOR THE COMMANDER



(Signature)

RITA SAGALYN
Division Director

This report has been reviewed by the ESD Public Affairs Office (PA) and is releasable to the National Technical Information Service (NTIS).

Qualified requestors may obtain additional copies from the Defense Technical Information Center. All others should apply to the National Technical Information Service.

If your address has changed, or if you wish to be removed from the mailing list, or if the addressee is no longer employed by your organization, please notify AFGL/DAA, Hanscom AFB, MA 01731. This will assist us in maintaining a current mailing list.

Do not return copies of this report unless contractual obligations or notices on a specific document requires that it be returned.

AD-A169466
REPORT DOCUMENTATION PAGE

1a REPORT SECURITY CLASSIFICATION UNCLASSIFIED			1b RESTRICTIVE MARKINGS		
2a SECURITY CLASSIFICATION AUTHORITY			3 DISTRIBUTION AVAILABILITY OF REPORT Approved for public release; distribution unlimited.		
2b DECLASSIFICATION/DOWNGRADING SCHEDULE N/A since UNCLASSIFIED					
4 PERFORMING ORGANIZATION REPORT NUMBER(S) SRI Project 4592			5 MONITORING ORGANIZATION REPORT NUMBER(S) AFGL-TR-86-0022		
6a NAME OF PERFORMING ORGANIZATION SPI International		6b OFFICE SYMBOL (if applicable)		7a NAME OF MONITORING ORGANIZATION Air Force Geophysics Laboratory (AFGL)	
6c ADDRESS (City, State, and ZIP Code) 333 Ravenswood Avenue Menlo Park, CA 94025		7b ADDRESS (City, State, and ZIP Code) Hanscom AFB, MA 01731			
8a NAME OF FUNDING/SPONSORING ORGANIZATION Electronic Systems Division		8b OFFICE SYMBOL (if applicable) PKR		9 PROCUREMENT INSTRUMENT IDENTIFICATION NUMBER F19628-82-K-0045	
8c ADDRESS (City, State, and ZIP Code) Air Force Systems Command Hanscom Air Force Base, MA 01731		10 SOURCE OF FUNDING NUMBERS			
		PROGRAM ELEMENT NO 61102F		PROJECT NO 2311	
				TASK NO G2	
				WORK UNIT ACCESSION NO EE	
11 TITLE (Include Security Classification) COORDINATED RADAR AND SATELLITE STUDIES OF IONOSPHERIC CURRENTS IN THE AURORAL ZONE AND POLAR CAP					
12 PERSONAL AUTHOR(S) Roland T. Tsunoda; Anne Q. Smith; John D. Kelly; Robert M. Robinson					
13a TYPE OF REPORT Final Technical		13b TIME COVERED FROM 9/1/82 TO 12/31/85		14 DATE OF REPORT (Year, Month, Day) 1985 December	
15 PAGE COUNT 40					
16 SUPPLEMENTARY NOTATION					
17 COSATI CODES			18 SUBJECT TERMS (Continue on reverse if necessary and identify by block number)		
FIELD	GROUP	SUB-GROUP			
17	02	1	Field-Aligned Currents, Incoherent-Scatter Radar		
20	09		Convection Electric Field, Satellite Magnetometer		
			High-Latitude Ionosphere (continued p. 2)		
19 ABSTRACT (Continue on reverse if necessary and identify by block number) An objective of the Air Force is to provide real-time surveillance or short-term predictions of the electrodynamic state of the ionosphere and magnetosphere. The desired approach is to obtain all necessary environmental information by remote sensing or by in-situ sampling from satellites; the necessary quantities include (1) electric fields, (2) ionospheric conductivities, and (3) field-aligned currents. Recently, a DMSP (Defense Meteorological Satellite Program) satellite has been launched (Flight 7) equipped with a triaxial fluxgate magnetometer. To qualify this type of instrument for participation in the above objective, an investigation was initiated to field-aligned currents estimated from two different approaches: (1) using magnetometer measurements made from the DMSP-F7 satellite and (2) using ionospheric measurements made by the Sondrestrom incoherent-scatter (continued p. 2)					
20 DISTRIBUTION AVAILABILITY OF ABSTRACT <input type="checkbox"/> UNCLASSIFIED UNLIMITED <input checked="" type="checkbox"/> SAME AS RPT <input type="checkbox"/> DTIC USERS			21 ABSTRACT SECURITY CLASSIFICATION UNCLASSIFIED		
22a NAME OF RESPONSIBLE INDIVIDUAL FREDERICK RICH			22b TELEPHONE (Include Area Code)		22c OFFICE SYMBOL AFGL/PHG

UNCLASSIFIED

SECURITY CLASSIFICATION OF THIS PAGE

18 SUBJECT TERMS (continued)

Polar Cap
Ionospheric Currents
Dayside Cleft
Auroral Zone

19. ABSTRACT (continued)

radar. We analyzed three events, when near simultaneous measurements were made by both instruments during satellite passes over the radar. Varying degrees of correlation were found in the derived field-aligned currents. In all three cases, the gross features measured by the two methods were similar. The differences are discussed in terms of measurement error, analysis approximations, and geophysical uncertainties.

UNCLASSIFIED

SECURITY CLASSIFICATION OF THIS PAGE

CONTENTS

LIST OF ILLUSTRATIONS.	v
I INTRODUCTION.	1
II ANALYSIS CONSIDERATIONS	5
A. Equations for Estimating FAC.	5
B. Magnetometer Measurements	7
C. Sondrestrom Radar Measurements.	8
III RESULTS	9
A. 16 April 1984 (1138 to 1142 UT)	9
B. 7 March 1984 (1133 to 1136 UT).	16
C. 11 December 1984 (1202 to 1204 UT).	25
IV SUMMARY	31
REFERENCES	33



Accession For	
NTIS CRA&I	<input checked="" type="checkbox"/>
DTIC TAB	<input type="checkbox"/>
Unannounced	<input type="checkbox"/>
Justification	
By	
Distribution /	
Availability Codes	
Dist	Avail and/or Special
A-1	

ILLUSTRATIONS

1	Satellite-radar geometry showing regions of field-aligned currents detected by each instrument, 16 April 1984.	10
2	DMSP magnetometer records showing magnetic perturbations produced by field-aligned currents, 16 April 1984.	12
3	Ionospheric electrodynamic parameters computed from radar measurements, 16 April 1984.	14
4	Satellite-radar geometry showing regions of field-aligned currents detected by each instrument, 7 March 1984	18
5	DMSP magnetometer records showing magnetic perturbations produced by field-aligned currents, 7 March 1984	19
6	Ionospheric electrodynamic parameters computed from radar measurements, 7 March 1984	21
7	The northward (geomagnetic) component of the electric field as a function of invariant latitude, 7 March 1984. . . .	23
8	Satellite-radar geometry showing regions of field-aligned currents detected by each instrument, 11 December 1983	26
9	DMSP magnetometer records showing magnetic perturbations produced by field-aligned currents, 11 December 1983	27
10	Ionospheric electrodynamic parameters computed from radar measurements, 11 December 1983	28
11	Comparison of northward ionospheric currents and eastward magnetic perturbations, as a function of invariant latitude, 11 December 1983	30

I INTRODUCTION

An objective of the Air Force is to provide real-time surveillance or short-term predictions on the electrodynamic state of the ionosphere and magnetosphere. The desired approach is to obtain all necessary environmental information by remote sensing or by in situ sampling from satellites: the necessary quantities include (1) electric fields, (2) ionospheric conductivities, and (3) field-aligned currents (FAC). Particle detectors (the SSJ/4 instrument) have been carried with the satellites in the Air Force's Defense Meteorological Satellite Program (DMSP) for many years [Hardy et al., 1979], and their use in estimating ionospheric conductivities has been demonstrated [e.g., McNeil and Hardy, 1984]. The DMSP-F7 (Flight 7) satellite (launched 18 November 1983) carries a triaxial fluxgate magnetometer (called the SSM instrument) in addition to the particle detector. The SSM instrument was placed on the DMSP-F7 spacecraft to prove that a scientific quality magnetometer could fly on operational satellites. (There was some doubt whether useful data could be obtained from a body-mounted sensor, in contrast to one mounted on a long boom.) Rich [1984] has recently described the excellent quality of the DMSP-F7 magnetometer data.

A next step is to evaluate the major assumptions or approximations that are often used to estimate FAC from magnetometer measurements. These include the following: (1) FAC regions can be approximated by infinite current sheets that extend in a generally east-west direction; and (2) magnetometer variations measured along the satellite trajectory represent a spatial FAC pattern that is invariant with time. These assumptions are in fact implicit in most reported FAC characteristics [e.g., Iijima and Potemra, 1976a,b, 1978].

A useful approach toward understanding the conditions under which such assumptions or approximations are valid is to compare estimates of FAC intensity using two independent means. For example, in a

preliminary analysis, Rich [1984] showed good but not perfect agreement in FAC intensities estimated from DMSP-F7 measurements of (1) particle precipitation characteristics with the SSJ/4 instrument and (2) magnetic variations with the SSM instrument. This lack of agreement indicates either that there are current carriers outside the energy range of the SSJ/4 instrument, or that there are other complicating factors. Another available instrument that is capable of determining FAC is the incoherent-scatter radar. A comparative analysis of satellite and radar results is useful because each technique is based on a different set of assumptions and approximations. Some degree of confidence in the results can be developed if consistent estimates of FAC can be derived from both techniques.

FAC intensity estimated from measurements made with the Chatanika incoherent-scatter radar have been compared with that from magnetometers on other satellites: eight events with the Triad satellite [Robinson et al., 1982] and two events with the S3-2 satellite [Vondrak and Rich, 1982]. In both investigations, FAC estimates were compared using data obtained from the diffuse auroral region in the premidnight sector. The convection electric field in this region was directed northward, with a large and relatively uniform amplitude. Consequently, the ionospheric closure of FAC seemed to be accommodated by a latitudinal gradient in ionospheric Pedersen conductivity (produced by diffuse precipitation of central plasma sheet electrons). In both of these investigations, downward (Region 2) FACs measured by the satellites were in reasonably good agreement with the radar results. The radar, however, did not provide sufficient latitudinal coverage to encompass the boundary between the Region 1 and Region 2 FAC sheets [e.g., Iijima and Potemra, 1976a].

Very little is yet known about the consistency of FAC estimates from satellite and radar measurements made in other time sectors and in the presence of discrete, precipitation produced structures. Unpublished results indicate that FAC estimates by the two techniques are not necessarily in good agreement in the presence of auroral arcs [Robinson, 1984].

For this investigation, we analyzed data from coordinated measurements made with the DMSP-F7 satellite and the incoherent-scatter radar located in Sondre Stromfjord, Greenland. The DMSP-F7 satellite is in a sun-synchronous orbit with its ascending node at 1030 local time. Consequently, with the Sondrestrom radar located at a latitude in the vicinity of the dayside auroral oval, this investigation allowed us to analyze relationships of FAC, electric fields, and ionospheric currents in the prenoon cleft region. This region is of considerable interest because of its differences with the evening diffuse auroral region. The prenoon sector is believed to be characterized by (1) ionization produced by solar illumination, (2) softer electron precipitation than in the evening sector, and (3) the possible presence of east-west electric fields associated with the "throat" region [Heelis et al., 1976; Heelis, 1984].

The results presented in this report include comparisons of FAC intensity derived from radar and satellite measurements made during three selected events. We found that electric-field gradients, rather than gradients in Pedersen conductivity, provide the primary means of ionospheric closure of FACs. The latter plays an increasingly larger role in the winter when solar illumination is absent. Good agreement was found in estimates of FAC intensity from the two techniques under conditions of distributed Pedersen conductivity. Serious disagreement was found when estimating FAC intensity in the vicinity of an auroral arc.

II ANALYSIS CONSIDERATIONS

A. Equations for Estimating FAC

We use a Cartesian coordinate system in which the X, Y, and Z axes correspond with geomagnetic east, geomagnetic north, and upward along geomagnetic field lines. This coordinate system is usually used in presenting incoherent-scatter radar results. On the other hand, the coordinate convention used for the DMSP-F7 data [Rich, 1984] is: +X, downward; +Y, forward; and +Z, horizontal cross-track. In the three events analyzed here, the satellite is northbound in the prenoon sector, and confined (more or less) to the local magnetic meridian plane. For these cases, the satellite Y-axis is aligned with geomagnetic north and the Z-axis is aligned with geomagnetic east.

The derivation of FAC intensity using magnetometer data that follows is similar to that presented by others [e.g., Smiddy et al., 1980; Vondrak and Rich, 1982]. We begin with Maxwell's equation, neglecting displacement currents

$$\nabla \times \underline{B} = \mu_0 \underline{j} \quad (1)$$

where μ_0 is the permeability of free space (1.257×10^{-6} H/m) and the other symbols have their usual meanings. (Underscored symbols indicate vector notation.) At altitudes above the E region, transverse ionospheric currents are negligible; therefore, Eq. (1) becomes

$$\partial B_y / \partial x - \partial B_x / \partial y = \mu_0 j_z \quad (2)$$

where we have replaced j_z by j_z . Equation (2) states that upward FAC is associated with a decrease in the eastward magnetic perturbation component (B_x) with increasing latitude, an increase in the northward magnetic perturbation component (B_y) with increase in eastward longitude, or both.

We next assume longitudinal uniformity, so that Eq. (2) becomes

$$\partial B_x / \partial y = -\mu_0 j_{\parallel} \quad . \quad (3)$$

This assumption is necessary because the satellite is in a polar orbit and, therefore, provides no information on longitudinal gradients. On the other hand, this assumption seems to be reasonably satisfied on the basis of results presented in the next section, as well as those by Robinson et al. [1982] and Vondrak and Rich [1982]. The assumed uniformity in longitude also implies that the FAC sheets are infinite in extent along the X-axis (east-west direction). A useful form of Eq. (3) for computing FAC intensity is given by

$$j_{\parallel} (\mu A/m^2) = -0.8 \partial B_x / \partial y (nT/km) \quad . \quad (4)$$

The FAC intensity is estimated from radar measurements by assuming a divergence-free total current, i.e.,

$$\nabla \cdot \underline{j} = 0 \quad (5)$$

or

$$\int (\partial j_x / \partial x + \partial j_y / \partial y) dz = -j_{\parallel} \quad . \quad (6)$$

If we assume that FACs are closed through the ionosphere by Pedersen currents [e.g., Sugiura et al., 1982], $j_x = \sigma_x E_x$, $j_y = \sigma_y E_y$, where σ is the ionospheric conductivity. Using this notation, Eq. (5) becomes

$$\partial / \partial x [\sigma_x E_x dz] + \partial / \partial y [\sigma_y E_y dz] = -j_{\parallel} \quad (7)$$

This assumed current closure is consistent with the infinite FAC sheet approximation. We further assume that $E_{\parallel} = 0$ and that E_x and E_y map along the z-axis (the geomagnetic field line),

$$\partial E_x / \partial x / \sigma_x dz + \partial E_y / \partial y / \sigma_y dz = -j_{\parallel}$$

or

$$\partial / \partial x (\int_x E_x) + \partial / \partial y (\int_y E_y) = -j_{\parallel} \quad (8)$$

Again, we assume longitudinal uniformity, which leaves

$$\partial / \partial y (\int_y E_y) = -j_{\parallel} \quad (9)$$

Equation (9) states that a downward FAC is accompanied by an increase in northward ionospheric current with increasing latitude. Note that the current gradient can be produced by contributions from gradients in either the field-line-integrated conductivity (or conductance), \int , or electric field. A useful form of Eq. (9) that can be used to compute FAC from radar measurements is

$$j_{\parallel} (\mu A / m^2) = -\partial / \partial y (\int_y E_y) (\text{mhos} \cdot \text{mV} / \text{m} / \text{km}) \quad (10)$$

B. Magnetometer Measurements

The magnetometer on the DMSP-F7 satellite was designed to measure changes in the geomagnetic field with a resolution of 12 nT at a rate of 20 samples/axis/s. Potential sources of magnetometer error include interference from other DMSP instruments and a possible misalignment of the sensor unit of up to 0.2° per axis [Rich, 1984]. For comparison, the S3-2 magnetometer data have a resolution of 5 nT at a rate of 32 samples/axis/second [Burke et al, 1980] and the Triad magnetometer data have a resolution of 12 nT at a rate of 2.25 samples/axis/second [Saflekos et al, 1978]. The magnetometer data used in this study and presented here represent one-second averages of data subtracted from the International Reference Magnetic Field (IGRF-80) model.

C. Sondreström Radar Measurements

Most of the radar data used in this report were obtained from north-south elevation scans. Mean line-of-sight ion velocities were computed by integrating constant-range data samples obtained typically over a 15-to-30-s period. For a scan rate of $0.3^\circ/\text{s}$, the means were obtained from 4.5° to 9° angular segments of the elevation scan. The two horizontal components of the electric field are computed by applying the ion-motion equation at two different altitudes, using height-dependent equations for the Pedersen and Hall mobilities to resolve the vector. Vertical electric fields are assumed negligible. The errors in using this method to derive the electric fields are discussed by de la Beaujardiere et al., [1977]. The horizontal current densities are then found by multiplying the radar-measured height-integrated Hall and Pedersen conductivities with the inferred electric fields. The altitude range of integration was 85 to 200 km.

III RESULTS

We present three comparisons of FACs estimated from satellite and radar data obtained in the local prenoon sector. The data were selected for analysis based on two criteria: (1) simple signatures of FACs in the DMSP-F7 magnetometer data and (2) minimal separation in time and space between satellite and radar measurements. The results are presented in order of increasing global magnetic activity, decreasing solar activity, and increasing solar zenith angle. This order of presentation results in FAC patterns that are, in addition to electric field gradients, increasingly determined by gradients in Pedersen conductance. In all three events, there appeared to be little evidence (in magnetograms recorded at Kiruna, Sweden) of substorm activity during satellite passes.

A. 16 April 1984 (1138 to 1142 UT)

The first event occurred on Day 107 around 0940 MLT, and was characterized by low global magnetic activity ($K_p = 1+$) and an E layer produced primarily by solar illumination (solar zenith angle = 67.7°). Because ionospheric conductances produced by solar illumination are relatively uniform, ionospheric closure of the FACs is associated with latitudinal variations in the electric field. The radar was operated in a three-scan cycle consisting of two elevation scans (south to north, and north to south), and an azimuth scan at 70° elevation angle. Each elevation scan was made at a true azimuth of 340° , and took seven minutes to complete. (The magnetic declination is about 320° true azimuth.) The lowest elevation angle at both ends of the scan was 25° . This scan cycle was repeated throughout an 8-hour period that included a DMSP-F7 pass near the radar.

The satellite-radar geometry and regions of FAC detected by satellite and radar are presented in Figure 1. The subsatellite position as

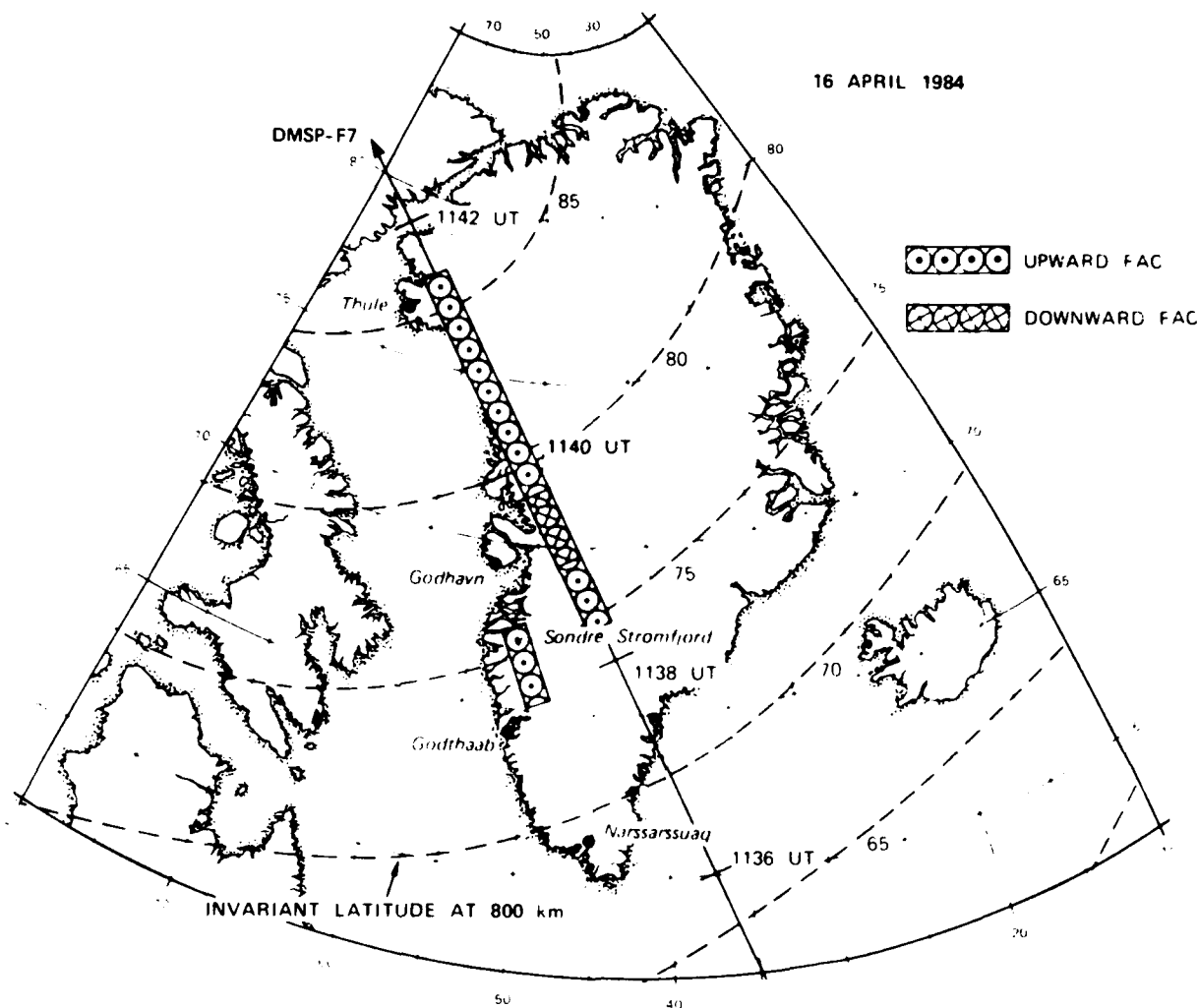


FIGURE 1 SATELLITE-RADAR GEOMETRY SHOWING REGIONS OF FIELD-ALIGNED CURRENTS DETECTED BY EACH INSTRUMENT, 16 APRIL 1984

a function of time is shown by a line with tick marks given at two-minute intervals. Regions of upward and downward FAC observed by satellite (at 830-km altitude) are denoted by circled dots and circled crosses, respectively. Similar symbols are used to denote regions of FAC detected by radar during an elevation scan made in near time conjunction with the satellite pass. [The radar FAC regions are referenced to an altitude near the Pedersen conductivity maximum (125 km). The

radar-derived FAC regions, therefore, need to be displaced equatorward by about a degree when they are compared to those derived by satellite measurements, or when estimating their corresponding invariant latitudes from Figure 1.] The northbound DMSP-F7 satellite passed about 280 km east of the radar. The trajectory of the DMSP-F7 satellite seen in Figure 1 is nearly perpendicular to the contours of constant invariant latitude (drawn for an altitude of 800 km) and nearly parallel to the radar scan. The radar scan was made between 1139 and 1146 universal time (UT), so the time coincidence in UT is nearly exact.

The in situ magnetometer measurements made from the DMSP-F7 satellite are presented in Figure 2. As described in Section II, the X, Y, and Z magnetometer coordinates correspond to the downward, forward, and cross-track directions from the satellite. Because the orbital plane of DMSP-F7 was essentially in the local magnetic meridian, the Z axis is directed eastward during ascending (northbound) passes, and the Y axis is directed northward. Magnetic perturbations that appear only in the Z-component, DB_z , can, therefore, be interpreted as east-west-aligned, infinite FAC sheets. If magnetic perturbations also appear in the Y component, DB_y , the FAC sheets are then interpreted as being tilted away from the east-west direction.

Magnetic perturbations are produced by (1) instrumental effects, (2) large-scale FAC regions, and (3) small-scale geophysical effects. For example, the bias changes in DB_z between 1133:30 and 1135:30 UT, and between 1155:00 and 1157:00 UT represent instrumental effects [see Rich, 1984 for details], and should be ignored. The large-scale FAC regions are seen in DB_z between 1138 and 1142 UT (in the prenoon local time sector), and between 1148 and 1150 UT (in the premidnight sector). Small-scale geophysical effects are seen as transient perturbations (or "spikes"), e.g., at 1138:45 UT and 1139:30 UT. These small-scale features are seen to differ from the regular "granularity" seen in the remainder of the DB_z trace. At least in some cases, these small-scale features are believed to be associated with auroral arcs. The DB_y component is seen to be relatively smooth, except for a negative deviation around 1139:15 UT, indicating that the FAC sheets are aligned more or less with constant invariant latitudes.

GMT-SEC	41520	41640	41760	41880	42000	42120	42240	42360	42480	42600	42720	42840	42960
GLAT	46.4	53.3	60.1	66.8	73.1	78.5	81.2	79.0	73.8	67.5	60.9	54.0	47.1
GLNG	330.6	327.5	323.4	317.4	307.4	287.6	249.5	209.1	187.7	177.1	170.6	166.5	163.3

FIGURE 2 DMSP MAGNETOMETER RECORDS SHOWING MAGNETIC PERTURBATIONS PRODUCED BY FIELD-ALIGNED CURRENTS, 16 APRIL 1984

The feature of interest here is the prenoon FAC signature. From Eq. (3) or (4), a negative (positive) slope in DB_z (as a function of increasing latitude, or UT) is a measure of upward (downward) FAC. The DB_z variations are consistent with the prenoon pattern of FAC reported by Iijima and Potemra [1976b], i.e., a Region 2 (upward) FAC at lowest latitudes, a Region 1 (downward) FAC at intermediate latitudes, and a cusp (upward) FAC at highest latitudes. Note that that DB_z trace returns to a baseline that is virtually identical to that seen before the FAC sheets appeared. This indicates that there is no net FAC [Sugiura and Potemra, 1976]. The absence of a net FAC and a relatively smooth DB_y trace are consistent with closure of FACs by meridional currents during this event.

To estimate FAC intensity from magnetometer data, a single slope was chosen to represent each DB_z variation; the FAC is, therefore, considered uniform across the linearly-fitted region for purposes of comparison with radar data. The estimated mean values for the upward (Region 2), downward (Region 1), and cusp FAC are $1.1 \mu A/m^2$, $2.0 \mu A/m^2$ and $0.8 \mu A/m^2$, respectively. In comparison, Iijima and Potemra [1978] found average values of 1.5 and $0.5 \mu A/m^2$ for Region 1 and Region 2 FAC intensities during quiet geomagnetic conditions ($AL < 100$ nT). The reversal from upward to downward FAC measured by the magnetometer occurred at 77.3° invariant latitude.

The radar results from corresponding measurements made during the DMSP-F7 pass are presented in Figure 3. The plasma density distribution measured during the elevation scan is shown in the top panel. Isodensity contours are used to describe the plasma density distribution; the contour interval is 2×10^4 el/cm³. A gray scale, in steps of 1×10^5 el/cm³ has also been used to accentuate the large-scale features. Plasma density in E layer is seen to be about 1×10^5 el/cm³ over a 200-km latitudinal extent centered over the radar, and decreases with distance away from the radar in both directions. The E-layer ionization was produced primarily by solar illumination with a slight local enhancement produced by particle precipitation.

1139.09 TO 1146.09 UT

16 APRIL 1984

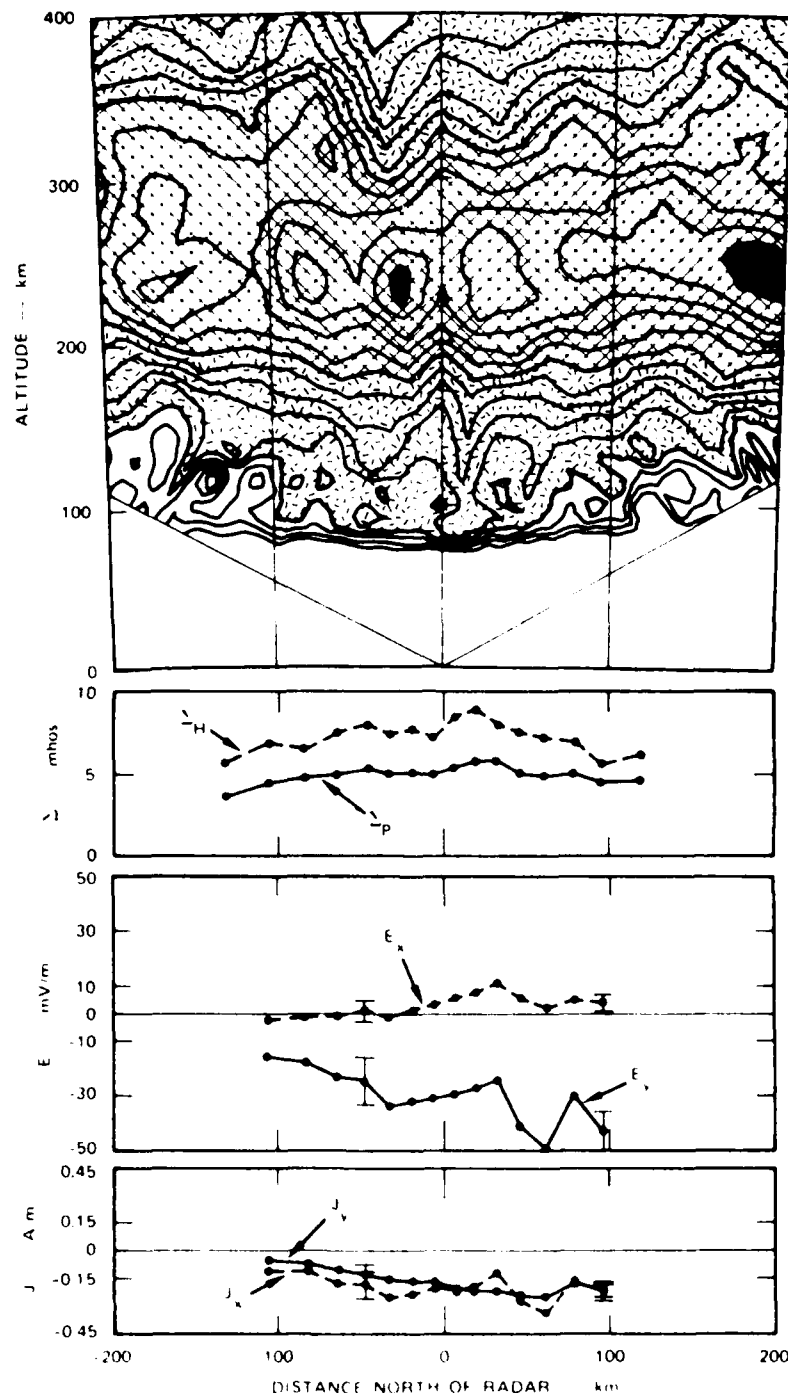


FIGURE 3 IONOSPHERIC ELECTRODYNAMIC PARAMETERS
COMPUTED FROM RADAR MEASUREMENTS,
16 APRIL 1984

The Pedersen and Hall conductances are presented in the second panel of Figure 3. The latitudinal extent is limited by the E-region coverage by the radar during the elevation scan. The Pedersen conductance (solid line) is relatively uniform with a slight bulge in the vicinity of the radar that is produced by localized particle precipitation. For a solar zenith angle of 67.7° (over the radar) and a 10.7-cm solar radio flux of $117.2 \times 10^{-22} \text{ W/m}^2/\text{Hz}$ (adjusted to 1 AU), the solar contribution to the Pedersen conductance is about 6 mhos [Robinson and Vondrak, 1984]; this amount represents the bulk of the ionospheric conductances seen in the second panel. Although the F-layer plasma density exceeded $3 \times 10^5 \text{ el/cm}^3$, it did not contribute significantly to the Pedersen conductance.

The two geomagnetic components of the electric field are presented in the third panel of Figure 3. The northward component of the electric field, E_y , is plotted with a solid line, and the eastward component, E_x , is plotted with a dashed line. E_y is directed southward, increasing in magnitude up to a latitude just north of the radar, and remained more or less constant with a value close to 40 mV/m at higher latitudes. A southward component is consistent with the presence of a westward Hall electrojet in the prenoon sector. The presence of a small eastward component is consistent with a gradual counterclockwise rotation of plasma flow direction with local time towards the antisunward direction in the noon sector. The confinement of electric-field variations to E_y is consistent with magnetometer data (Figure 2) that indicate essentially east-west aligned FAC sheets, and with closure of the FAC sheets through the ionosphere via meridional Pedersen currents.

Finally, the ionospheric currents are presented in the fourth panel of Figure 3. The northward component, J_y is seen to nearly mirror the variations of the southward electric field. The southward current represents the Pedersen current that provides the ionospheric closure for the FAC sheets. The result is an equatorward-directed Pedersen current that increases with latitude until about 60 km north of the radar, then remains more or less constant at higher latitudes. The estimated strength of the mean upward FAC obtained from radar data is $0.9 \text{ } \mu\text{A/m}^2$.

(Both the downward FAC in Region 1 and upward cusp FAC seen by the satellite are beyond the radar's field of view.) The magnitude of FAC estimated from radar measurements are in very good agreement with those estimated from magnetometer measurements.

If we assume that the equatorward boundary of the upward (Region 2) FAC sheet is coincident with the latitude where the northward ionospheric current goes to zero, we can infer from Figure 3 that the boundary must have been located close to 73° invariant latitude. Referring back to Figure 1, we see that the boundary is situated about 1.5° equatorward of the FAC boundary estimated from magnetometer data. Assuming that the satellite was 280 km east of the radar, we find that the FAC boundary must have been tilted counterclockwise about 30° from the east-west direction. This tilt is about a factor of two larger than indicated by the ratio of the electric field components but has the proper sense. This tilt, if real, is not in accord with infinite FAC sheets that are aligned in east-west direction. The FAC sheets must either (1) be tilted in the same manner as the FAC boundary and ratio of the electric field components or (2) be associated with longitudinal gradients.

B. 7 March 1984 (1133 to 1136 UT)

The second event occurred on Day 67 around 0935 MLT, and was characterized by moderate global magnetic activity ($K_p = 3+$) and an E layer produced by nearly equal contributions from solar illumination (solar zenith angle = 83.5°) and particle precipitation. Conductivity variations were further complicated by the presence of an auroral arc; therefore, the FAC pattern in this case was affected by gradients in both Pedersen conductance and electric field.

The radar was operated in a standard "World Day" mode, consisting of (1) 11 fixed-beam positions, (2) a south-to-north elevation scan at 333° true azimuth, and (3) an east-to-west elevation scan at 63° true azimuth. It takes 15 min to execute the 11-position mode, and 5 min to execute each of the elevation scans. The 11 beam positions are

distributed in latitude about the radar magnetic meridian so that vector electric fields can be computed from pairs or triads of these point measurements. Electric fields derived from 11-position data use only F-region measurements. The lowest elevation angle used in the elevation scans is 30° , 5° higher than used for the first event.

The radar-satellite geometry and regions of FAC detected by the two instruments are presented in Figure 4. The satellite passed in the vicinity of the Sondrestrom radar between 1133 and 1137 UT; the radar scan occurred between 1132 and 1137 UT, so again the coincidence in UT was nearly exact. The northbound satellite passed less than 350 km east of the radar at nearest approach, and in a plane approximately parallel to the radar elevation scan. The apparent discrepancies, in Figure 4, between the large-scale FAC regions determined by the two techniques are discussed below.

The magnetometer data for this event are presented in Figure 5. The V-shaped variations in the DB_z component that occurred between 1133:30 and 1135:45 UT occurred in the local prenoon sector. A small-scale perturbation is imbedded within the V-shaped region suggesting the presence of an auroral arc. This pattern differs from the first event (Figure 2) in that a cusp FAC region was not detected. The widths of the FAC sheets in Region 1 and Region 2 in both prenoon and premidnight sectors are wider than those seen in Figure 2. The increased widths are consistent with a higher level of magnetic activity that prevailed during this event. The V-shaped variation is also reflected in the DB_y component, suggesting that the FAC sheets are not aligned with satellite coordinates.

The DB_z component is seen to vary slowly from about 70° invariant latitude to about 73.5° where the slope steepens and becomes more or less linear. The latitudinal extent and location of the linear-sloped segment is seen in Figure 4 to be in good agreement with the FAC region determined by radar. Only the steeper portion within a few degrees of the reversal was considered for comparison with the radar, as the radar could not view the regions further south. The estimated mean values for

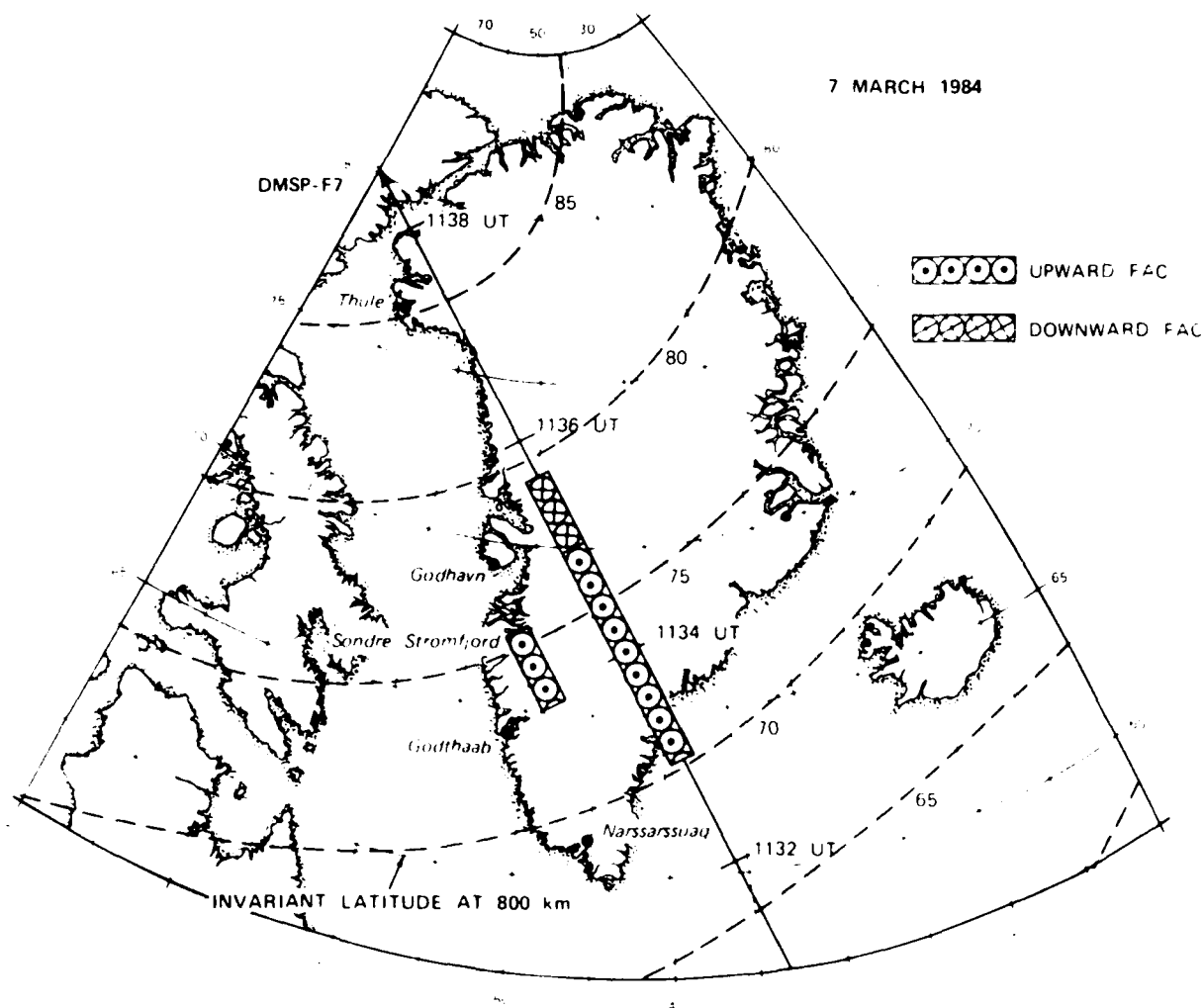


FIGURE 4 SATELLITE-RADAR GEOMETRY SHOWING REGIONS OF FIELD-ALIGNED CURRENTS DETECTED BY EACH INSTRUMENT, 7 MARCH 1984

7 MARCH 1984

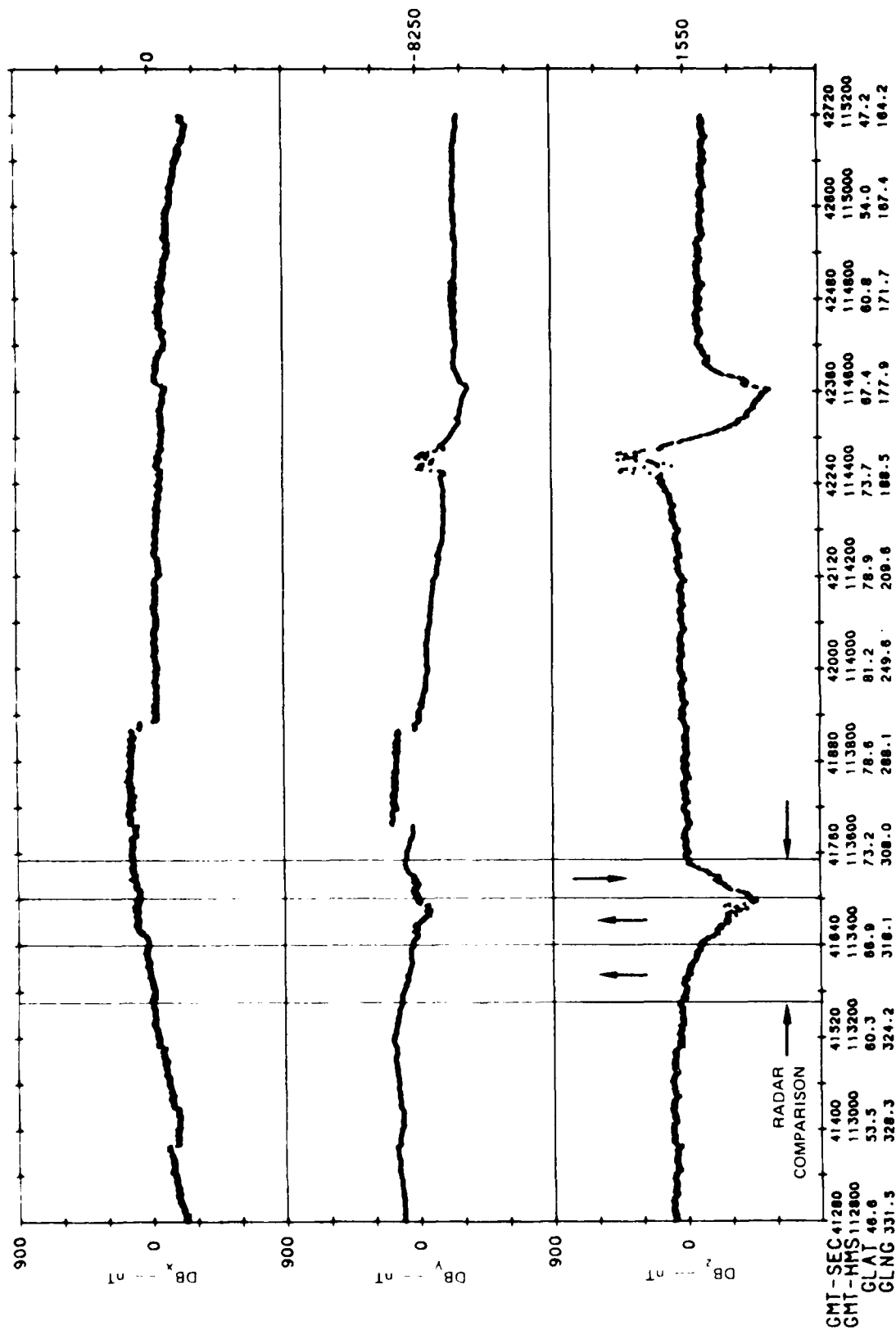


FIGURE 5 DMSP MAGNETOMETER RECORDS SHOWING MAGNETIC PERTURBATIONS PRODUCED BY FIELD-ALIGNED CURRENTS, 7 MARCH 1984

the upward and downward field-aligned currents measured by the satellite magnetometer are $1.4 \mu\text{A}/\text{m}^2$ and $1.0 \mu\text{A}/\text{m}^2$, respectively. These values are in good agreement with those reported by Iijima and Potemra [1978].

Results obtained from the elevation-scan data are presented in Figure 6. The latitudinal coverage is slightly less than available in the first event because higher start and stop elevation angles were used compared to those during the first event. The plasma density distribution, seen in the top panel, differs markedly from that in the first event. Rather than a uniform, solar-illuminated E layer with minimal ionization effects from particle precipitation, we find two E-layer features that precipitation produced: (1) a diffuse E layer equatorward of the radar, and (2) an auroral arc poleward of the radar. Note that the peak of the diffuse E layer is close to 150-km altitude, considerably higher than found in the night sector. The peak plasma density in the auroral arc is at an even higher altitude.

The latitudinal variations in E-layer plasma density is clearly reflected in the Hall and Pedersen conductances presented in the second panel of Figure 6. The minimum in the Pedersen conductance occurred in the gap between the diffuse E layer and the auroral arc. The minimum value of about 3 mhos is consistent with the solar illumination conditions (solar zenith angle = 83.5° , $10.7 \text{ cm solar radio flux of } 105 \times 10^{-22} \text{ W}/\text{m}^2/\text{Hz}$) that existed at the time.

The electric-field components are presented in the third panel of Figure 6. The meridional component is seen to be directed southward and increases with latitude. This pattern is similar to that found in the first event. The increase, however, is not monotonic, with a sharp local (southward) enhancement around 20 km north of the radar.

The components of the ionospheric currents are presented in the fourth panel of Figure 6. The north-south component is seen to reflect the variations in both the electric field and the Pedersen conductance. To the south of the radar, the slope of J_y is reduced by the decrease in Pedersen conductance with latitude. To the north, the slope of J_y is

1132 06 TO 1137 05 UT

7 MARCH 1984

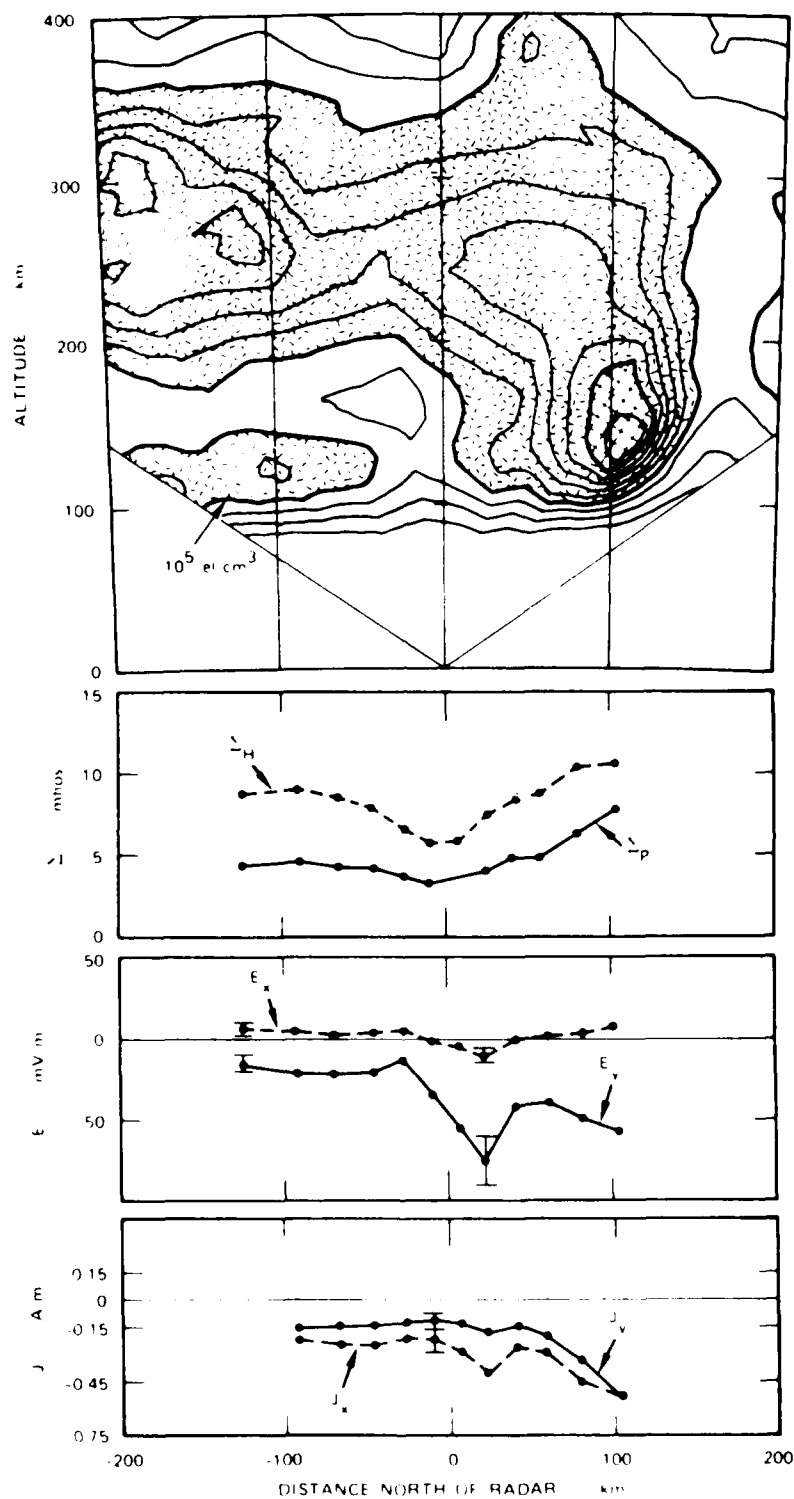


FIGURE 6 IONOSPHERIC ELECTRODYNAMIC PARAMETERS
COMPUTED FROM RADAR MEASUREMENTS,
7 MARCH 1984

enhanced by the increase in Pedersen conductance associated with the auroral arc. The choice of a "best" slope to characterize J_y over Region 2 is not as clear as in the previous case. To the south of the radar the negative J_y slope is less steep than further north. This does not reflect the similar shape of the satellite DB_z component, however, as this slope variation occurs over a smaller scale. For purposes of comparison, the slope was taken over the entire region rather than the steeper portion to the north of the radar. The radar-estimated value of the upward FAC is $6.5 \mu A/m^2$, so there is considerable discrepancy in the calculated magnitude of the upward current.

The electric field variations have been found in many cases to reflect the variations of FAC [e.g., Sugiura et al., 1982]; therefore, it is useful to examine the electric-field pattern derived from radar measurements. The 11-position mode which uses only F-region measurements provides a measure of the vector electric field over a broader latitudinal region than the elevation scan mode. The electric-field pattern derived from 11-position and elevation scan data is shown in Figure 7. Circled dots connected by line segments represent estimates of the electric field derived from 11-position data. The numbers indicate the order in which the data were collected. The fourth data segment, shown by crosses, was derived from elevation scan data. We find a very systematic pattern in which E_y is directed southward, increasing in magnitude from zero at 71° invariant latitude to about 80 mV/m around 76° invariant latitude. The electric-field strength remained close to 75 mV/m from 76° to 77.5° , then decreased in strength until about 79° invariant latitude. As can be seen, the data are well represented by a three-segment, linear least-squares fit. (A quadratic fit to the negatively sloped region has also been included for comparing the goodness of fit.)

This gross pattern of electric field variation is virtually identical with the FAC pattern derived from magnetometer measurements that were presented in Figure 4. A general agreement is also expected in the sense that auroral arcs represent only small-scale perturbations in the ionospheric current pattern.

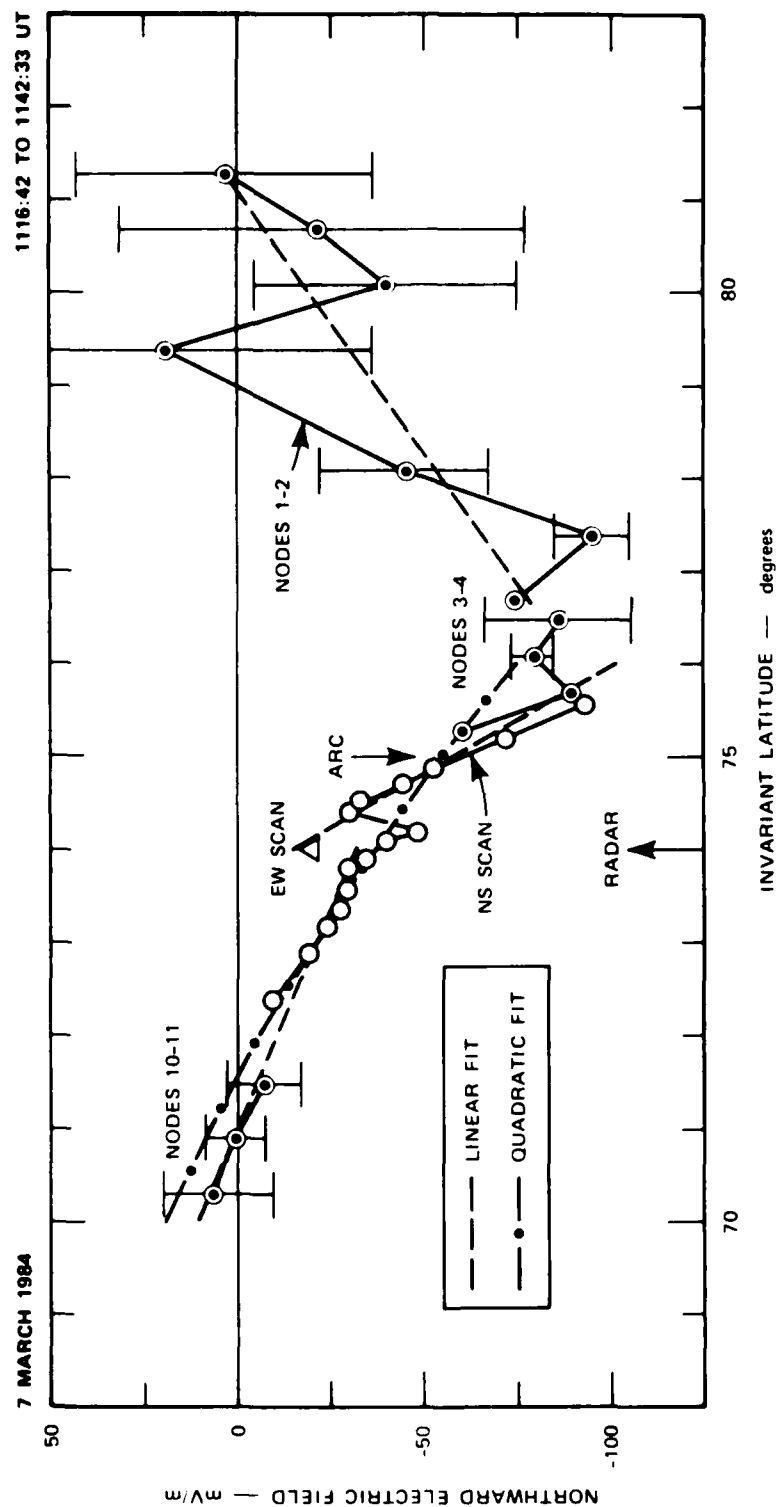


FIGURE 7 THE NORTHWARD (GEOMAGNETIC) COMPONENT OF THE ELECTRIC FIELD AS A FUNCTION OF INVARIANT LATITUDE, 7 MARCH 1984

Using the mean slopes derived from the three-segment, linear least-squares fit to the data, we can estimate the FAC intensity associated with each region. At low latitudes, $\partial E_y / \partial y = -1 \times 10^{-7} \text{ V/m}^2$. The Pedersen conductance in this region is controlled by solar illumination and diffuse particle precipitation, as seen in Figure 6 (and from DMSP-F7 particle measurements). On this basis, we estimate that the Pedersen conductance is uniform over this region with a value of about 4 mhos (Figure 6). We, therefore, obtain an upward FAC intensity of $0.4 \text{ } \mu\text{A/m}^2$ and obtain $0.3 \text{ } \mu\text{A/m}^2$ from the magnetometer data.

In the vicinity of the auroral arc, we find $\partial E_y / \partial y = -4 \times 10^{-7} \text{ V/m}^2$ from a local linear fit to the data. We then used the following parameters estimated from Figure 6: $E_y = -50 \text{ mV/m}$, $\Sigma_y = 6.5 \text{ mhos}$, $\partial \Sigma_y / \partial y = 6 \times 10^{-5} \text{ mhos/m}$; to estimate a FAC intensity of $5.6 \text{ } \mu\text{A/m}^2$. This value is in good agreement with our earlier estimate of $6.5 \text{ } \mu\text{A/m}^2$. About half of this FAC intensity is associated with the gradient in Pedersen conductance. On the poleward side of the arc, the gradient in Pedersen conductance is negative; therefore, we expect a strong reduction in FAC intensity there.

Poleward and well beyond the auroral arc, the electric field gradient is positive with a value of $1.6 \times 10^{-7} \text{ V/m}^2$. If we use a FAC intensity of about $1.0 \text{ } \mu\text{A/m}^2$ (estimated from the magnetometer data) and assume no gradients in Pedersen conductance, the required Pedersen conductance is about 6 mhos. The actual Pedersen conductance would be lower if we allow for the presence of a decreasing Pedersen conductance with latitude. Qualitatively, this is expected from reduced particle precipitation in the polar cap (relative to the auroral oval), and an increase in solar zenith angle with latitude.

In summary, we found excellent agreement between satellite and radar measurements of FAC intensity in that portion of Region 2 associated with diffuse particle precipitation. In the high-latitude segment occupied by an auroral arc, the FAC estimated from radar measurements was about a factor of four greater than that estimated from satellite measurements. In Region 1, the estimated Pedersen conductance required

to match satellite and radar measurements seemed to be reasonable in value.

C. 11 December 1983 (1202 to 1204 UT)

The third event occurred on Day 345 around 1003 MLT and was characterized by high global magnetic activity, with Kp values of 4(0900 to 1200 UT) and 6(1200 to 1500 UT), and a dark E layer (solar zenith angle = 97.2°). Under these conditions, ionospheric dynamics is controlled by large convection electric fields and a Pedersen conductance that depends primarily on particle precipitation.

The radar was operated in a mode consisting of successive elevation scans down to 30° elevation angle. Each elevation took 7 min to complete. During the DMSP-F7 pass, the scan plane was directed 316° true azimuth, about 4° west of the nominal magnetic meridian direction of 320° true azimuth.

The radar-satellite geometry and regions of FAC are presented in Figure 8. The spatial coincidence for this event is the best of the three events investigated in this paper. The northbound satellite pass was nearly directly over the radar. FAC were detected by magnetometer from 1202:45 to 1203:40 UT. The radar scan was made between 1200 and 1207 UT.

The magnetometer data for this event are presented in Figure 9. The DB_z variations, in this case, has an inverted-V shape. There are two possible interpretations: (1) the variations represent Region 1 and Region 2 FAC that are representative of the postnoon sector, or (2) the variations represent Region 1 and cusp FAC from the prenoon sector. Without choosing between these two interpretations, McDiarmid et al. [1978] showed that inverted-V shapes (or eastward magnetic perturbations) occurred when the B_y component of the interplanetary magnetic field was positive, and V shapes (or westward magnetic perturbations) occurred when B_y was negative. Similar results were obtained by Wilhelm et al. [1978]. The estimated mean values for the downward and upward field-aligned currents are $1.7 \mu A/m^2$ and $2.3 \mu A/m^2$, respectively.

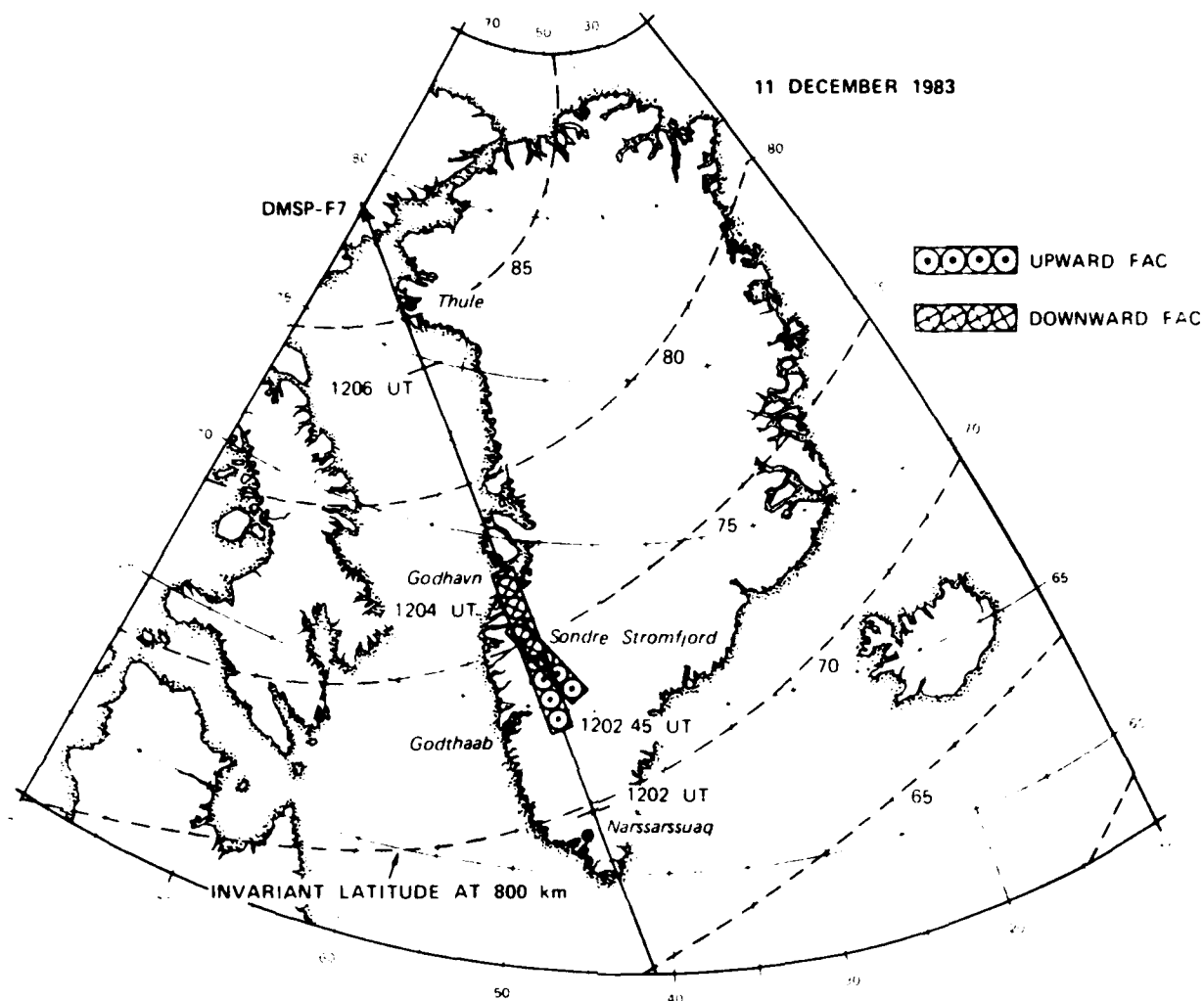
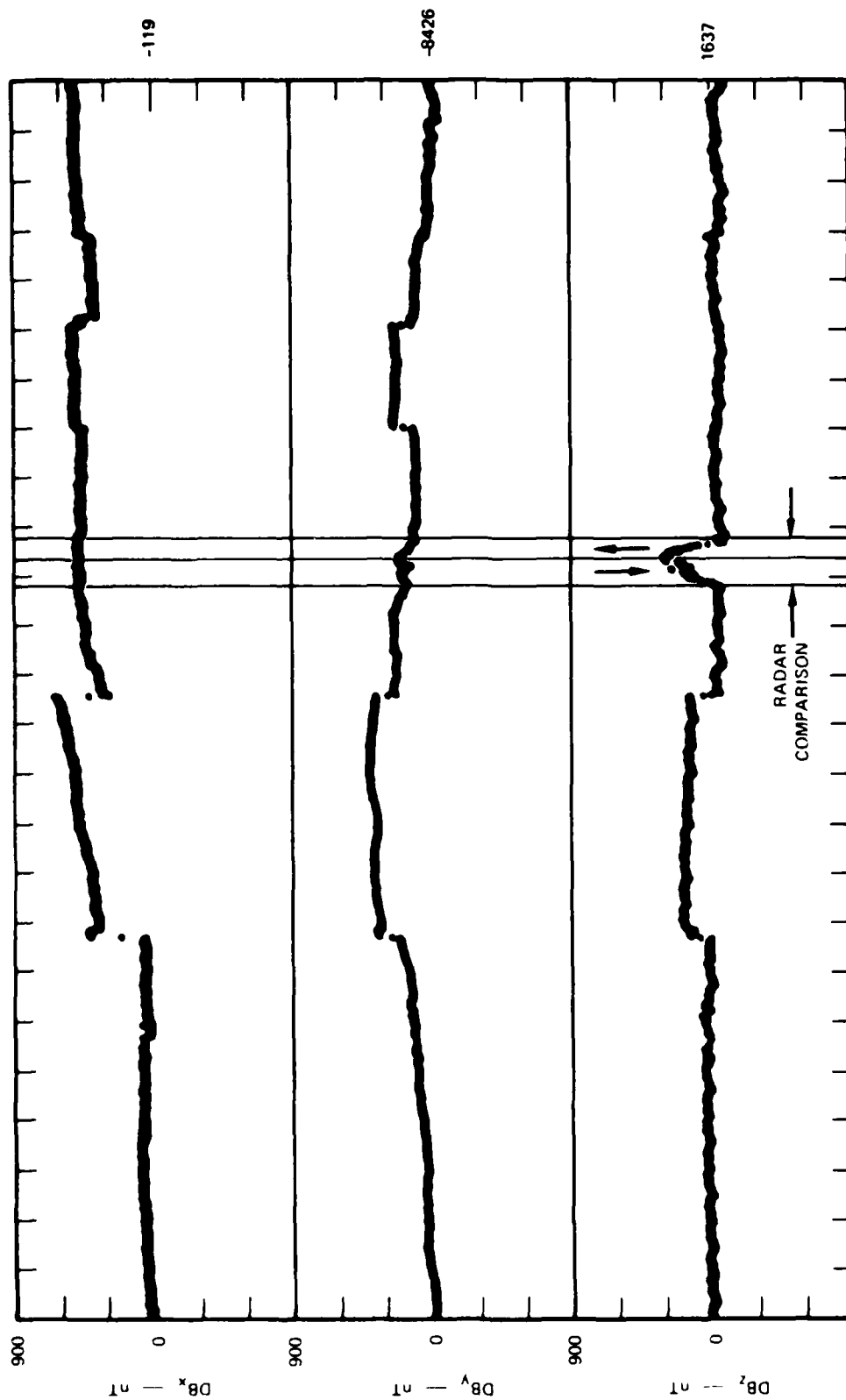


FIGURE 8 SATELLITE-RADAR GEOMETRY SHOWING REGIONS OF FIELD-ALIGNED CURRENTS DETECTED BY EACH INSTRUMENT, 11 DECEMBER 1983

The radar results are presented in Figure 10. The plasma densities in the top panel are much lower than in the two previous cases, reflecting the winter conditions. There is virtually no solar contribution to E-layer ionization because of a solar zenith angle of 97.2° . A narrow, precipitation-produced E layer seems to be centered overhead of the radar with a peak plasma density of 4 to 6×10^4 el/cm^3 . This value is half that seen in the first two events. The only other feature is a

11 DECEMBER 1983



GMT-HMS	1148	1150	1152	1154	1156	1158	1200	1202	1204	1206	1208	1210	1212
GLAT	13.5	20.5	27.5	34.5	41.5	48.4	55.3	62.1	68.7	74.8	79.7	81.0	77.7
GLNG	333.4	331.7	329.9	328.0	325.7	323.1	319.7	315.2	308.3	296.4	272.0	229.7	194.6

FIGURE 9 DMSP MAGNETOMETER RECORDS SHOWING MAGNETIC PERTURBATIONS PRODUCED BY FIELD-ALIGNED CURRENTS, 11 DECEMBER 1983

1132 06 TO 1137 05 UT

11 DECEMBER 1983

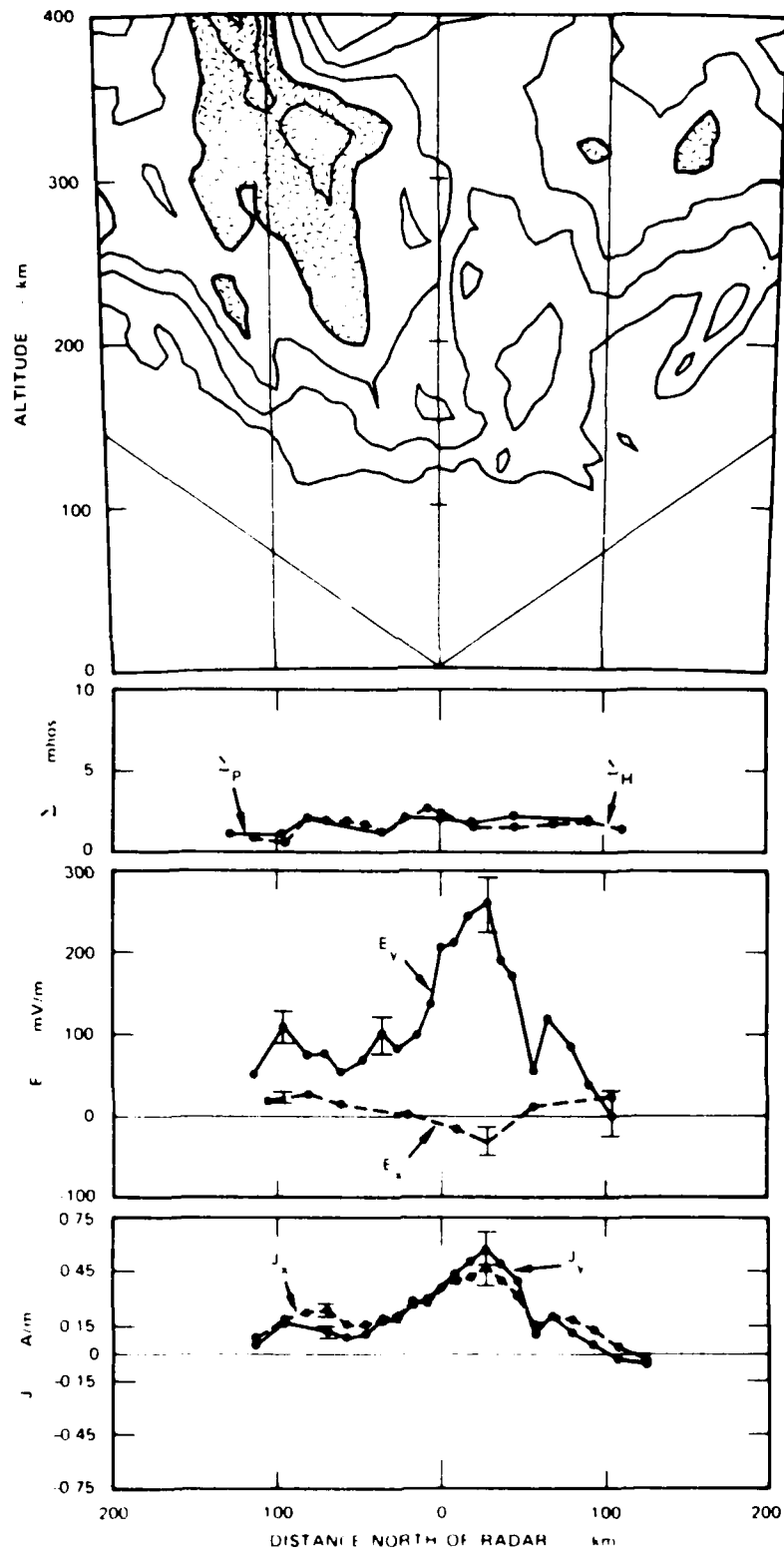


FIGURE 10 IONOSPHERIC ELECTRODYNAMIC PARAMETERS
COMPUTED FROM RADAR MEASUREMENTS,
11 DECEMBER 1983

patch of ionization in the F layer; but that too is less dense than its counterparts in the previous two events. As expected from the low plasma densities, the Hall and Pedersen conductances shown in the second panel are seen to be correspondingly low.

The electric-field components are plotted in the third panel of Figure 10. Again, the eastward component is small and without significant structure. The northward component, however, is sharply peaked just poleward of the radar. The most surprising feature is a peak value that is in excess of 250 mV/m. This value is one of the largest ever observed by incoherent-scatter radar. A northward electric field in this time sector would correspond to antisunward convection if associated with the morning convection cell. It is conceivable that the afternoon cell had penetrated into the morning sector during this event.

The calculated ionospheric currents are presented in the bottom panel of Figure 10. The shape is clearly dominated by large electric field variations but also extended in latitude to some degree by the taper in ionospheric conductance. For the radar, the estimated values of FAC intensity are $2.6 \mu\text{A}/\text{m}^2$ and $3.1 \mu\text{A}/\text{m}^2$ for the downward and upward FAC sheets, respectively.

Figure 11 shows the gross DB_z and radar J_y variations. For this case with excellent time and spatial coincidence, the agreement in location of the reversal from upward to downward current sheets appears nearly exact.

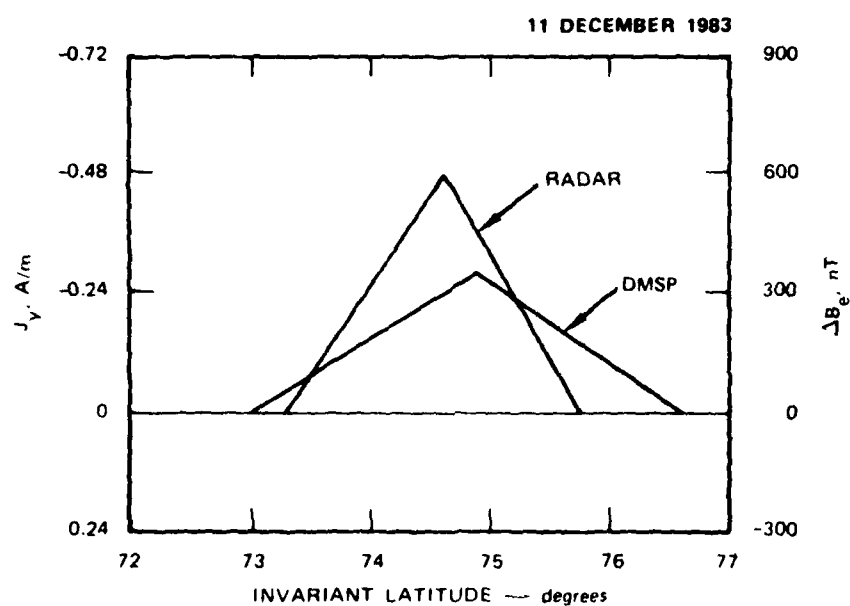


FIGURE 11 COMPARISON OF NORTHWARD IONOSPHERIC CURRENTS AND EASTWARD MAGNETIC PERTURBATIONS, AS A FUNCTION OF INVARIANT LATITUDE, 11 DECEMBER 1983

IV SUMMARY

We have presented comparisons of FAC derived by two independent techniques. In the first event (16 April 1984), only a portion of the region 2 FAC sheet was within the field of view of the radar. The FAC intensity determined for that portion was found to be in good agreement with that determined from magnetometer measurements. The equatorward boundary of the Region 2 FAC (as determined by radar) appeared to be located about 2° further south than that determined by satellite.

Similar radar coverage occurred for the second event (7 March 1984). Again, only the Region 2 FAC region was visible within the radar elevation scan. To augment this comparison, we examined the electric field pattern available from 11-position radar data taken during this World Day. The electric field pattern was found to be in excellent agreement with the entire FAC region including Region 1 and Region 2 FAC sheets. In the third event (11 December 1983), both Regions 1 and 2 FAC sheets were situated within the radar field of view, including the FAC reversal boundary. The FAC intensities as well as the reversal location derived from radar data were in good agreement with those derived from satellite measurements.

It is emphasized that both methods used to estimate the field-aligned current are very rough. For the satellite and the radar a "best guess" slope was estimated and used in the calculation. For the three cases presented here the slope of the satellite data varied smoothly, so approximating the slope this way should not produce any gross errors. For the radar data, there was much more measured local variation; alternate slopes could be used, which could substantially change the values presented here.

The best agreement in the location of the boundary between Region 1 and Region 2 FAC was for the case in which the satellite passed closest

to the radar. In both of the other cases the satellite passed to the east of the radar at the same UT as the radar elevation scan, but at a later magnetic local time. Holzworth and Meng [1975] show the location of the auroral oval increasingly poleward with increasing MLT over the morning sector. This may explain much of the discrepancy in invariant latitude for both 16 April and 7 March 1984; for both cases the satellite pass occurred approximately one half hour later in MLT.

Overall, considering the potential sources of error in both the radar and satellite measurement, geophysical uncertainty, and the assumptions used to infer the FAC from both sources of measured data, we find excellent agreement. Improvements in FAC estimates can be made by analysis of satellite imagery of auroral forms to see if the assumption of longitudinal uniformity is reasonable.

REFERENCES

- Burke, W. J., D. A. Hardy, F. J. Rich, M. C. Kelley, M. Smiddy, B. Shuman, R. C. Sagalyn, R. P. Vancour, P. J. L. Widman, and S. T. Lai, Electrodynamic structure of the late evening sector of the auroral zone, J. Geophys. Res., 85, 1179, 1980.
- de la Beaujardiere, O., R. Vondrak, and M. Baron, Radar observations of electric fields and currents associated with auroral arcs, J. Geophys. Res., 82, 5051, 1977.
- Hardy, D. A., M. S. Gussenhoven, A. Huber, The precipitating electron detectors (SSJ/3) for the block 5D/flights 2-5 DMSP satellites: calibration and data presentation, Scientific Interim Report, AFGL-TR-79-0210, Project 7601, Air Force Geophysics Laboratory, Hanscom Air Force Base, MA 01731 (September 1979). ADA083136
- Heelis, R. A., The effects of interplanetary magnetic field orientation on dayside high-latitude ionospheric convection, J. Geophys. Res., 89, 2873, 1984.
- Heelis, R. A., W. B. Hanson, and J. L. Burch, Ion convection velocity reversals in the dayside cleft, J. Geophys. Res., 81, 3803, 1976.
- Holzworth, R.H. and C. I. Meng, Mathematical representation of the auroral oval, Geophys. Res. Letters, 2, 377, 1975.
- Iijima, T., and T. A. Potemra, The amplitude distribution of field-aligned currents at northern high latitudes observed by Triad, J. Geophys. Res., 81, 2165, 1976a.
- Iijima, T., and T. A. Potemra, Field-aligned currents in the dayside cusp observed by Triad, J. Geophys. Res., 81, 5971, 1976b.
- Iijima, T., and T. A. Potemra, Large-scale characteristics of field-aligned currents associated with substorms, J. Geophys. Res., 83, 599, 1978.
- McDiarmid, I. B., J. R. Burrows, and M. D. Wilson, Magnetic field perturbations in the dayside cleft and their relationship to the IMF, J. Geophys. Res., 83, 5753, 1978b.
- McNeil, W. J. and D. A. Hardy, Private Communication.

- Rich, F. J., Fluxgate Magnetometer (SSM) for the Defense Meteorological Satellite Program (DMSP), Air Force Geophysics Laboratory Report No. AFGL-TR-84-0225 IP, No. 326, 1984. ADAl55229
- Robinson, R. M., Private Communication, Lockheed Palo Alto Research Laboratory, Palo Alto, CA (1984).
- Robinson, R. M., and R. R. Vondrak, Measurements of E region ionization and conductivity produced by solar illumination at high latitudes, J. Geophys. Res., 89, 3951, 1984.
- Robinson, R. M., R. R. Vondrak, and T. A. Potemra, Electrodynamic properties of the evening sector ionosphere within the region 2 field-aligned current sheet, J. Geophys. Res., 87, 731, 1982.
- Saflekos, N. A., T. A. Potemra, and T. Iijima, Small-scale transverse magnetic disturbances in the polar regions observed by Triad, J. Geophys. Res., 83, 1493, 1978.
- Smiddy, M., W. J. Burke, M. C. Kelley, N. A. Saflekos, M. S. Gussenhoven, D. A. Hardy, and F. J. Rich, Effects of high-latitude conductivity on observed convection electric fields and Birkeland currents, J. Geophys. Res., 85, 6811, 1980.
- Sugiura, M., and T. A. Potemra, Net field-aligned currents observed by Triad, J. Geophys. Res., 81, 2155, 1976.
- Sugiura, M., N. C. Maynard, W. H. Farthing, J. P. Heppner, B. G. Ledley, and L. J. Cahill, Jr., Initial results on the correlation between the magnetic and electric fields observed from the DE-2 satellite in the field-aligned current regions, Geophys. Res. Lett., 9, 985, 1982.
- Vondrak, R. R. and F. J. Rich, Simultaneous Chatanika Radar and S3-2 satellite measurements of ionospheric electrodynamics in the diffuse aurora, J. Geophys. Res., 87, 6173, 1982.
- Wilhjelm, J., E. Friis-Christiansen, and T. A. Potemra, The relationship between ionospheric and field-aligned currents in the dayside cusp, J. Geophys. Res., 83, 5586, 1978.

END

DTIC

7-86